Polarization multi-parametric imaging method for the inspection of cervix cell

Weiping Liu[a,1], Jichuan Xiong[a,1], Juan Liu[a,1], Jing Zhu[b], Jinlian Hu[c], Lianping Hou[d], John H. Marsh[d], Muhua Yi[e], and Xuefeng Liu[a,*]

[a]*School of Electronic and Optical Engineering, Nanjing University of Science and Technology, 200 Xiaolingwei, Nanjing, 210094, China*

[b]*Jiangsu Key Laboratory for Pharmacology and Safety Evaluation of Chinese Materia Medica, School of Pharmacy, Nanjing University of Chinese Medicine, Nanjing, China*

[c]*Department of Biomedical Engineering, City University of Hong Kong, Hong Kong SAR 999077, China*

[d]*James Watt School of Engineering, University of Glasgow, Glasgow, G12 8QQ, UK*

[e]*Department of Pathology, Affiliated Dongguan People's Hospital, Southern Medical University, Dongguan 523059, China*

[1]*These authors contributed equally to this work*

E-mail: liuxf_1956@sina.com

Abstract

Accurate identification of the shape and texture properties of cervical cell nuclei and cytoplasm in the pap smear test is crucial for the diagnosis of cervical cancer. Fast and high-precision polarization modulation in the Polarization Indirect Microscopic Imaging (PIMI) is achieved by utilizing a liquid crystal polarization rotator. Imaging results of cervical cells show that the PIMI method can resolve detailed fine structural features of a cervical cell which are invisible in conventional microscopy. It also demonstrated the ability of embossed three-dimensional visualization as that in differential interference contrast microscopy (DIC), but with finer structural features.

Keywords

Polarization modulation; Cervix cell; Microscopic imaging

1. Introduction

The Papanicolaou (Pap) smear test is a manual screening procedure in which cells gathered from the cervix are smeared on a glass slide for microscopic examination [1-3]. It is used to detect precancerous changes in cervical cells based on color and shape characteristics of the

nucleus and cytoplasm. The Pap test has been the most effective cancer screening test ever and remains an important method for detecting the precursor lesions of cervical cancer. Many factors influence the sensitivity of the Pap test and, therefore, the reliability of the diagnosis. The test is greatly impacted by the quality of sampling and smearing [4]. The desire for reliable early diagnosis as well as difficulties in the manual screening process have led to the development of microscopies that offer high resolving power with fast imaging speed and accuracy to increase the speed and sensitivity of the diagnosis [1,5,6].

A variety of optical microscopies is available now for visual inspections of cells. By staining or tagging the biological tissues with dyes, fluorescent microscopes are method most commonly used for cell imaging [7,8], especially in differentiating of degenerate cells in a cell colony or sub-cellular components. However, the application of fluorescent microscopies is limited due to the optical toxicity and pollution of most labels to the organism. Label-free optical microscopies also have a broad field of applications in cell visualization. Phase-contrast microscopy [9], Differential Interference Contrast microscopy (DIC) [10], and interference reflection microscopy [11] are widely used to observe structure and motion in unstained living cells and isolated organelles and have been standard in laboratories since their invention. In addition, polarization-based imaging methods have also shown great potential in detecting structural and optical information about the tissues and cells [12-16]. As a result of their capability of obtaining abundant structural information of the tissue, polarization techniques are promising techniques for early screening and identification of cancers [17-26]. Here, we propose a fast polarization-based multi-parametric method, Polarization Indirect Microscopic Imaging (PIMI), for the inspection of cervical cells with nano-structural resolving power and sensitivity.

Recently, it has been demonstrated that the PIMI method, with its multi-parametric images, can be used to obtain rich detailed features of sub-cellular structures [27]. By measuring and filtering the distribution of the far-field optical scattering, PIMI can reveal high resolution nanoscale anisotropic structures using precisely modulated incident polarization [28,29]. This measurement scheme is mainly taking advantage of the high sensitivity of the polarization states of scattered photons to the anisotropic structures of material, especially when the sample shows abrupt variations of dimension and refractive index at the location where the photons are scattered.

In this paper, the PIMI method is applied to the observation of cervical cells. A Liquid Crystal Polarization Rotator (LCPR) is utilized for providing precise polarization modulation at a high speed. Through controlling the voltage of LCPR, each polarization state

can be modulated in 0.1 second and the whole measurement of PIMI would only cost about 1 second. Compared with the dual modulation way and 30 different states of polarization (SOPs) in Y. Wang's work [23], the system of PIMI is comparatively simpler, only using one modulation element and 10 SOPs. With PIMI method, not only the detailed fine structural features of the cervical cell, but the subcellular organelles of the cervical cell (such as mitochondria) can also be resolved in different illumination modes. Comparisons between the DIC and PIMI methods indicate that PIMI images not only to some degree obtain a similar embossed three-dimensional visual effect as the DIC images but also show greater capability in distinguishing the contour structures of cells. This approach can be applied in the Pap smear test to provide higher reliability and sensitivity of cell analysis and diagnosis, and also opens an opportunity for assisting in the diagnosis of other various cancer tissues.

2. System configuration and sample preparation

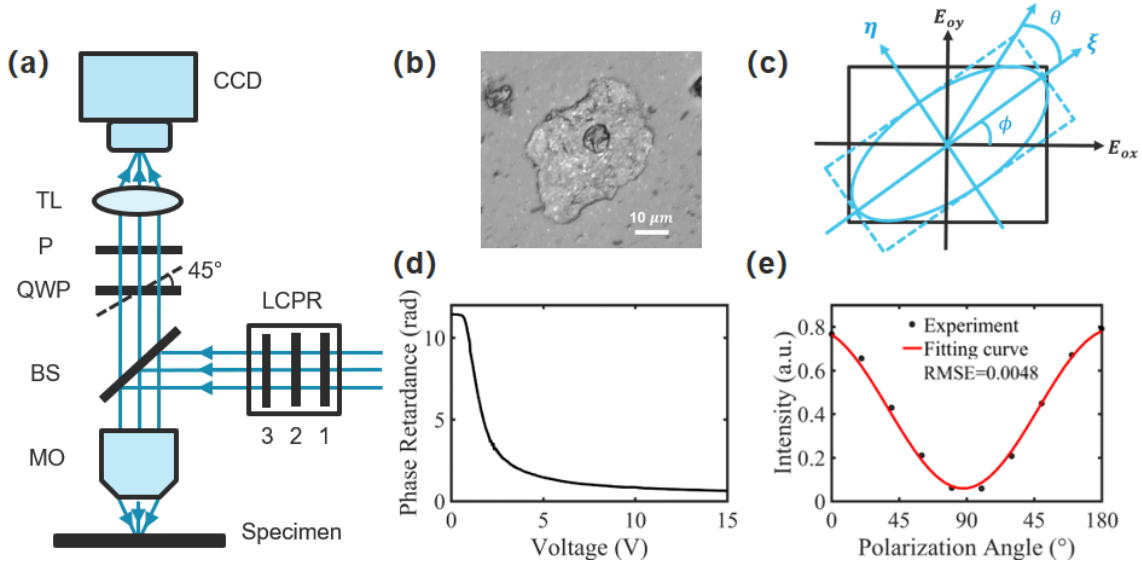

Fig. 1. (a) PIMI system configuration, TL: Tube Lens, P: Polarizer, QWP: Quarter Waveplate, BS: Beam Splitter, MO: Microscopic Objective, LCPR: Liquid Crystal Polarization Rotator, consisting of 1: Polarizer, 2: Liquid Crystal Variable Retarder and 3: Quarter Waveplate. (b) Single cervical cell imaged by a Conventional Microscope (CM). (c). Polarization ellipse representation, where E_{ox} and E_{oy} are the horizontal and vertical components of the electric field, ϕ is the azimuthal angle with respect to the slow vibration axis i.e. E_{ox} axis, θ is the polarization angle. (d) Phase retardation curve of Liquid Crystal Variable Retarder, the phase retardation varies with the modulated voltage. (e) Calibration curve of Liquid Crystal Polarization Rotator (LCPR), the polarization angle of incident light was modulated from 0° to 180° by LCPR with an angle period of the 18°.

2.1 System configuration

The PIMI system was built by making use of the basic optical path of a conventional microscope as shown in Fig. 1(a). By incorporating a Liquid Crystal Polarization Rotator

(LCPR) and a highly sensitive CCD (PiA2400-17gm, Basler) with a pixel resolution of 3.45 μm, images under illumination light with different polarization angles can be obtained. In particular, the LCPR consists of a polarizer, a Liquid Crystal Variable Retarder (LCVR) and a quarter waveplate, in which the LCVR can produce a retardation phase of more than 10 rad as shown in Fig. 1(d). The polarization angle of the incident light can be precisely modulated through the LCPR with a modulation accuracy > 99%, as shown in Fig. 1(e). During the PIMI measurement, the linear polarization angle of the illumination light is rapidly modulated from 0° to 360° within one minute. All images using conventional microscopy and PIMI were carried out with an illumination wavelength of 532 nm.

2.2 Sample preparation

Glass slide was pre-labeled with date and cervical scraping smear. The specimens were fixed in 95% alcohol first, then was scraped on glass slide for two times. The surface was wiped off the excess blood with the filter paper or wet gauze. All of these smears stained with rapid ultrafast Pap test.

3. Theory of PIMI method

The details of the measurement principle of PIMI were previously reported by the group [28,29]. In contrast to conventional microscopy, in a PIMI measurement, structural information related to anisotropic features in the sample can be collected by the CCD when the illuminating beam with different polarization angles impinges on the sample. Through the Jones model, the intensity variation at each spatial point covered by the PSF can be formulated as Eq. (1), and the PIMI parameters $sin\delta$ and ϕ can be extracted from it [28-30].

$$I_i = \frac{1}{2} I_0 [1 + sin\delta sin2(\theta_i - \phi)] \quad (1)$$

where I_i (the subscript i indicates the number of polarization rotation angles) represents pixel intensity, I_0 is incident light amplitude, $sin\delta$ is the sine of the phase difference between E_{ox} and E_{oy}, θ is the incident polarization angle and ϕ is the angle between the slow axis and E_{ox} axis.

By expanding Eq. (1) trigonometrically, it can be reformulated in the following form:

$$I_i = a_0 + a_1 sin2\theta_i + a_2 cos2\theta_i, \quad (2)$$

$$a_0 = \frac{1}{2} I_0,\ a_1 = \frac{1}{2} I_0 sin\delta cos2\phi,\ a_2 = -\frac{1}{2} I_0 sin\delta sin2\phi, \quad (3)$$

Using the precisely controlled LCPR, the incident polarization angle θ_i can be modulated from zero to 360°, with a total number of steps N = 360°/18°, and a_0, a_1 and a_2 can be calculated as (The polarization aberration caused by the beam splitter and high NA objective were already calibrated and compensated, seen in Supplementary materials):

$$a_0 = \sum_{i=1}^{N} \frac{1}{N} I_i,\ a_1 = \sum_{i=1}^{N} \frac{2}{N} I_i sin2\theta_i,\ a_2 = \sum_{i=1}^{N} \frac{2}{N} I_i cos2\theta_i, \quad (4)$$

The desired PIMI parameters can be finally obtained from the above equations:

$$I_{dp} = a_0,\ sin\delta = \frac{\sqrt{a_1^2+a_2^2}}{a_0},\ \phi = \frac{1}{2}\arccos\left(\frac{a_1}{\sqrt{a_1^2+a_2^2}}\right) \quad (5)$$

By modulating the polarization state of the incident optical field, PIMI images can reveal detailed minute structural characteristics of the sample under measurement. Resolution test targets were used for calibrating the resolution of the Conventional Microscopy (CM) and PIMI system as shown in Fig. 2. Fig. 2(b-d) shows a small knife-edge area imaged by CM and PIMI methods. As can be seen, the I_{dp} image is less noisy than the CM image and the ϕ image is more sensitive to abrupt changes, which are all consistent with the intensity curves shown in Fig. 2(e-g). The Modulation Transfer Function (MTF) was also calculated as shown in Fig. 2(h). The MTF curve of the ϕ image is much wider than that of the CM image, showing that the ϕ image has a higher spatial resolution than the CM image.

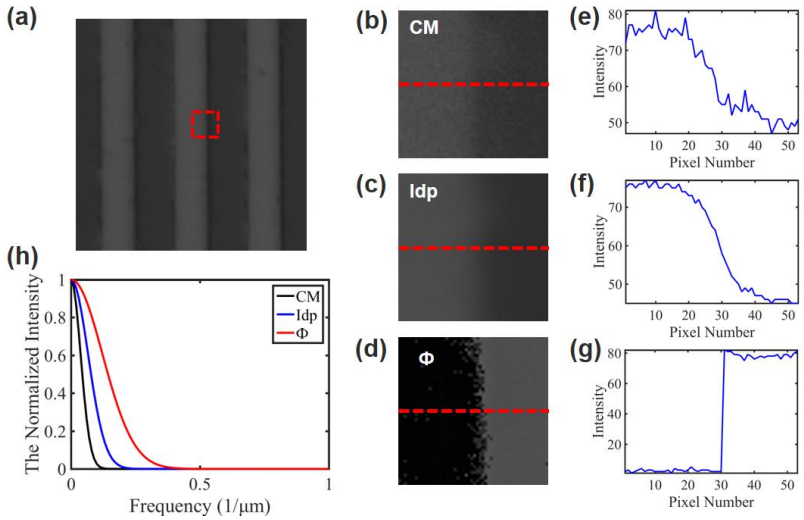

Fig. 2. (a) Resolution test targets under 100× magnification. (b) The dashed rectangle part in (a), taken with the Conventional Microscope (CM). (c) & (d) The same position as (b) taken with the PIMI method. (e-g) Intensity profiles across the dashed red lines in (b-d). (h) Modulation Transfer Function (MTF) curves calculated from (e-g).

4. Results and Discussion

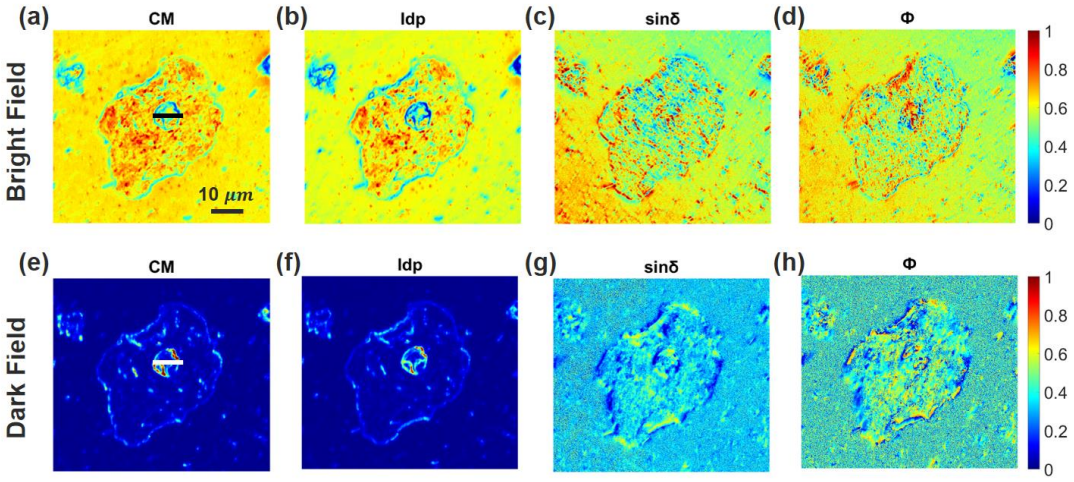

Fig. 3. (a-d) CM and PIMI images taken under bright field illumination, (e-h) CM and PIMI images taken under dark field illumination.

Experiments under different illumination conditions were carried out with a 50× objective as shown in Fig. 3. The top row shows comparisons between CM and PIMI results in the bright field illumination mode and the bottom row shows comparisons between CM and PIMI results under dark field illumination. The $sin\delta$ and ϕ images reveal more detailed features than the CM images, especially in the region of the nucleus of the cervical cell. Also, the $sin\delta$ and ϕ images are capable of resolving the wrinkles on the surface of the cervical cell. Structural variations in the $sin\delta$ and ϕ images are revealed more clearly than that in CM. Different from the CM dark field image, which only shows the boundaries of cell and nucleus, the $sin\delta$ and ϕ dark field images also resolve fine structure within the cell.

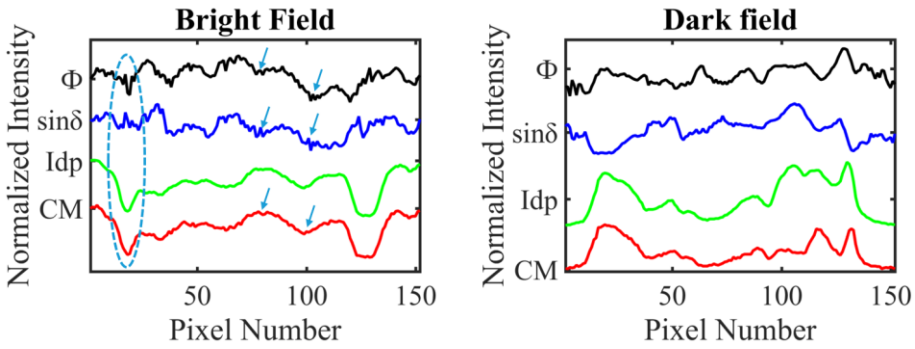

Fig. 4. Comparisons of intensity profiles across the nucleus of a cervical cell. Results taken under bright field illumination (left) and results taken under dark field illumination (right).

For further analysis, intensity profiles of all images along the short lines across the nucleus of the cervical cell, as marked in Fig. 3 (a) and (e), are plotted in Fig. 4. As can be seen, the intensity variations in the PIMI images in both illumination modes contain more features related to the nucleus compared to those in the CM images. As indicated by the dashed ellipse in the left graph of Fig. 4, which represents the boundary area of the cell nucleus, the intensity

curves of the $sin\delta$ and ϕ images show sharper and narrower peaks. Also, even finer features are revealed in PIMI results, as marked with the arrows, which are almost invisible in the curves of the CM image.

To make the visibility of the images comparable, the entire nucleus of a cervical cell imaged by CM and PIMI are illustrated in Fig. 5(c-e). As can be seen, $\sin\delta$ and ϕ images show more detailed structural information in the inner part of the nucleus, while the CM image shows little information about the contents of the nucleus. Figure 5(b) plots the Point Spread Function (PSF) of one boundary of the nucleus in CM and PIMI images, as marked by the short black line in Fig. 5(c). The Full Width at Half Maximum (FWHM) of the ϕ curve is about 60 nm, which is much more accurate than that of the CM image (about 210 nm). All the results indicate that the PIMI results are more sensitive in resolving the detailed structure of the nucleus and its contents. It is known that among the many morphological changes occurring in cancer cells, nuclear atypia is one of the most important, including changes in the nuclear size and shape, numbers and sizes of nucleoli, and chromatin texture [31-33]. As mentioned previously, with PIMI parameters, not only the detailed fine structural features of the cervical cell, but the subcellular organelles of the cervical cell (such as mitochondria) can also be resolved (see details in Supplementary materials). The above results indicate that the reliability and sensitivity of cell diagnosis could be better improved by utilizing the PIMI method.

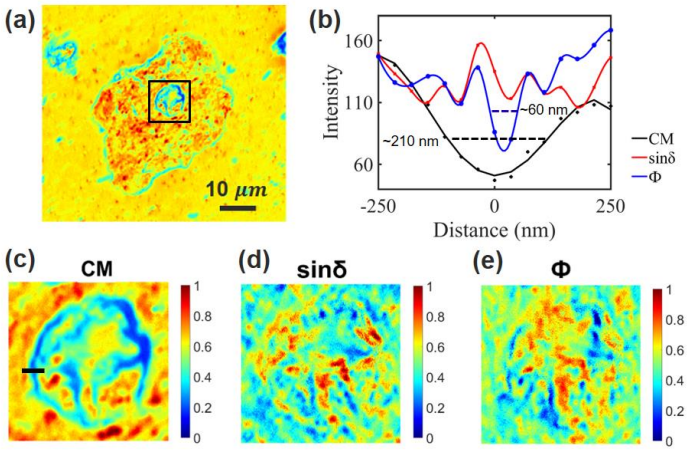

Fig. 5. (a) Cervical cell imaged by CM under bright field illumination. (b) Comparison between intensity profiles of CM, $sin\delta$ and ϕ along the black line marked in (c). (c-e) Enlarged nucleus of cervical cells imaged by CM and PIMI methods, in the region marked by the rectangle in (a).

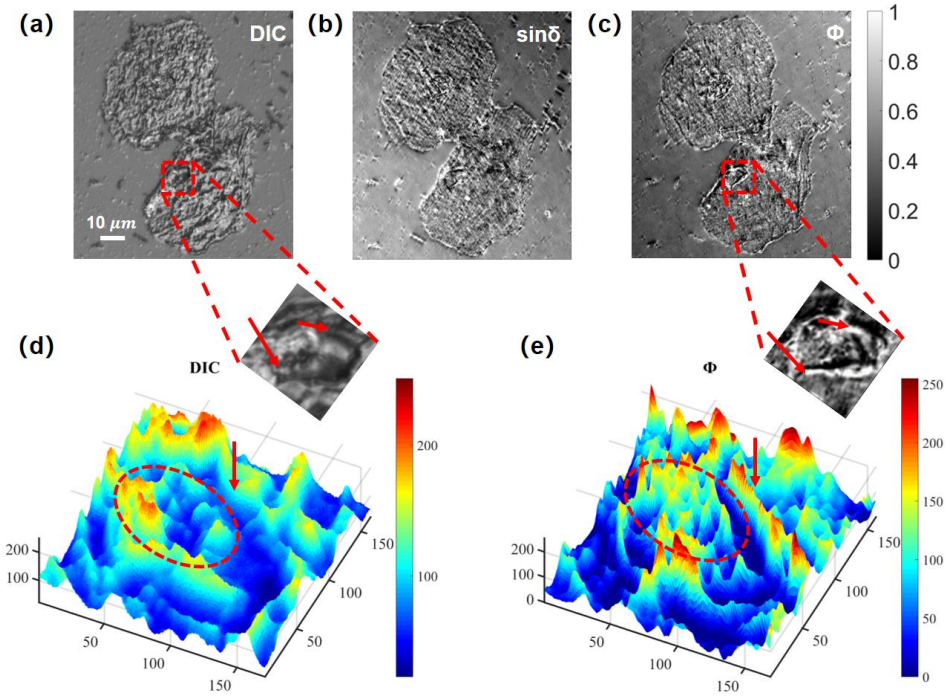

Fig. 6. (a-c) Comparison among DIC image, $sin\delta$ image, and ϕ image, (d) 3-dimension image of the enlarged nucleus in (a), (e) 3-dimension image of the enlarged nucleus in (c).

Comparisons between DIC microscopy and the PIMI method were also carried out by imaging the cervical cell, as shown in Fig. 6(a-c). As can be observed, PIMI images and DIC images all show the ability to resolve structural features of a cervical cell. It is also can be seen that the $sin\delta$ and ϕ images show a similar embossed three-dimensional visual effect to that of DIC images, especially in areas exhibiting abrupt structural changes such as boundaries of cell and nucleus and other line-shaped features. Figure 6(d) and (e) are three-dimensional images of a selected nucleus, as marked with dashed rectangles in Fig. 6(a) and (c). As can be seen, the contour structures of the cell nucleus in the ϕ image are clearer than in the DIC image, especially for the boundaries of nucleus marked with arrows. Also, the inner part of the nucleus in the ϕ image exhibits more distinct and richer structures than that in the DIC image as marked with a dashed ellipse.

5. Conclusion

In summary, it has been demonstrated that the PIMI method can provide much more information than CM images in cell analysis and diagnosis. It is more sensitive and reliable in visualizing cervical cells, especially in resolving the morphologies of whole-cell and sub-cellular structures with different biomechanical and structural properties, such as boundaries between the nucleus and cytoplasm. The application of a liquid crystal polarization rotator enables polarization modulation imaging with high precision and speed. The PIMI method reveals much more detailed nano-scale features of the nucleus in cervical cells and has

proved that the resolving power of PIMI is about 3 times that of CM. Comparisons between the DIC and PIMI methods indicate that PIMI images cannot only obtain a similar embossed three-dimensional visual effect as DIC images but also show greater capability in distinguishing the contour structures of cells. This approach can be applied to the Pap smear test to provide higher reliability and sensitivity of diagnosis, and also opens an opportunity for assisting in the diagnosis of other cancer tissues.

Declaration of competing interest

The authors declare that they have no known competing financial interests or personal relationships that could have appeared to influence the work reported in this paper.

Acknowledgments

This work was supported by the National Major Scientific Instruments and Equipment Development Project under Grant No.61827814, Beijing Natural Science Foundation under Grant No.Z190018, the Fundamental Research Funds for the Central Universities under Grant No.30920010011 and the Ministry of Education collaborative project. It is also supported by the UK Engineering and Physical Sciences Research Council (Grant EP/R042578/1).

References

1) A. Gençtav, S. Aksoy, and S. Önder, Unsupervised segmentation and classification of cervical cell images, Pattern Recognit. 45 (2012) 4151.
2) C. Bergmeir, M. G. Silvente, and J. M. Benítez, Segmentation of cervical cell nuclei in high-resolution microscopic images: A new algorithm and a web-based software framework, Comput. Methods Programs Biomed. 107 (2012) 497.
3) K. Aslı, and S. Aksoy, Segmentation of Cervical Cell Images, in *20th International Conference on Pattern Recognition. IEEE* (2010).
4) X. Hun, and L. Bai, Synthesis of Folate Conjugated Fluorescent Nanoparticle Probe and Its Application in Cervical Cancer Cell Imaging, Anal. Lett. 42 (2009) 2280.
5) E. Bengtsson, Computerized cell image analysis: past, present, and future, in *Proceedings of 13th Scandinavian Conference on Image Analysis* 395 (2003).
6) E. Bengtsson, Recognizing signs of malignancy—the quest for computer assisted cancer screening and diagnosis systems, in *IEEE International Conference on Computational Intelligence and Computing Research* (2010).
7) J. Wiedenmann, F. Oswald, G. U. Nienhaus, Fluorescent proteins for live cell imaging:

Opportunities, limitations, and challenges, IUBMB Life 61 (2009) 1029.

8) K. Nienhaus, and G. U. Nienhaus, Fluorescent proteins for live-cell imaging with super-resolution, Chem. Soc. Rev. 43 (2014) 1088.
9) F. Zernike, Phase contrast, a new method for the microscopic observation of transparent objects, Physica 9 (1942) 686.
10) R. D. Allen, G. B. David, and G. Z. Nomarski, The zeiss-Nomarski differential interference equipment for transmitted-light microscopy, Z. Wiss. Mikrosk. 69 (1969) 193.
11) A. S. G. Curtis, The mechanism of adhesion of cells to glass: a study by interference reflection microscopy, J. Cell Biol. 20 (1964) 199.
12) Y. Zhao, M. Reda, K. Feng, P. Zhang, G. Cheng, Z. Ren, S. G. Kong, S. Su, H. Huang, and J. Zang, Detecting Giant Cell Tumor of Bone Lesions using Mueller Matrix Polarization Microscopic Imaging and Multi-parameters Fusion Network, IEEE Sens. J. 99 (2020) 1.
13) R. S. Gurjar, V. Backman, L. T. Perelman, I. Georgakoudi, K. Badizadegan, I. Itzkan, R. R. Dasari, and M. S. Feld, Imaging human epithelial properties with polarized light-scattering spectroscopy, Nat. Med. 7 (2001) 1245.
14) S. L. Jacques, J. C. Ramella-Roman, and K. Lee, Imaging skin pathology with polarized light, J. Biomed. Opt. 7 (2002) 329.
15) L. Shen, Y. Zhao, Q. Peng, J. C. Chan, and S. G. Kong, An Iterative Image Dehazing Method with Polarization, IEEE Trans. Multimedia 1 (2018) 1.
16) H. Zhao, Q. Chen, U. Klimach, Y. K. Zou, and J. Xuan, Polarization imaging sensor for cell and tissue imaging and diagnostics, Proc. SPIE 6380 (2006) 06.
17) L. Qiu, D. K. Pleskow, R. Chuttani, E. Vitkin, J. Leyden, N. Ozden, S. Itani, L. Guo, A. Sacks, J. D. Goldsmith, M. D. Modell, E. B. Hanlon, I. Itzkan, and L. T. Perelman, Multispectral scanning during endoscopy guides biopsy of dysplasia in Barrett's esophagus, Nat. Med. 16 (2010) 603.
18) V. Backman, M. B. Wallace, L. T. Perelman, J. T. Arendt, R. Gurjar, M. G. Muller, Q. Zhang, G. Zonios, E. Kline, T. McGillican, S. Shapshay, T. Valdez, K. Badizadegan, J. M. Crawford, M. Fitzmaurice, S. Kabani, H. S. Levin, M. Seiler, R. R. Dasari, I. Itzkan, J. Van Dam, and M. S. Feld, Detection of preinvasive cancer cells, Nature 406 (2000) 35.
19) N. Ghosh, and I. A. Vitkin, Tissue polarimetry: concepts, challenges, applications, and outlook, J. Biomed. Opt. 16 (2011) 110801.
20) B. Kunnen, C. Macdonald, A. Doronin, S. Jacques, M. Eccles, and I. Meglinski, Application of circularly polarized light for non-invasive diagnosis of cancerous tissues and turbid tissue-like scattering media, J. Biophotonics 8 (2015) 317.

21) Y. Zhao, L. Zhang, and Q. Pan, Spectropolarimetric imaging for pathological analysis of skin, Appl. Opt. 48 (2009) 236.
22) M. Zaffar, A. Pradhan, Mapping of retardance, diattenuation and polarizance vector on Poincare sphere for diagnosis and classification of cervical precancer, J. Biophotonics 13 (2020) 1.
23) Y. Wang, H. He, J. Chang, N. Zeng, S. Liu, M. Li, and H. Ma, Differentiating characteristic microstructural features of cancerous tissues using Mueller matrix microscope, Micron 79 (2015) 8.
24) M. Zaffar, G. R. Sahoo, and A. Pradhan, Different orders of scattering through time-resolved Mueller matrix imaging estimates of pre-malignancy in human cervical tissues, Appl. Optics 59 (2020) 4286.
25) C. He, H. He, J. Chang, Y. Dong, S. Liu, N. Zeng, Y. He, and H. Ma, Characterizing microstructures of cancerous tissues using multispectral transformed Mueller matrix polarization parameters, Biomed. Opt. Express 6 (2015) 2934.
26) P. Li, H. R. Lee, S. Chandel, C. Lotz, F. K. G. Becker, S. Dembski, R. Ossikovski, H. Ma, and T. Novikova, Analysis of tissue microstructure with Mueller microscopy: logarithmic decomposition and Monte Carlo modeling, J. Biomed. Opt. 25 (2020) 1.
27) W. Liu, J. Xiong, H. Zhang, X. Liu, G. Liu, and H. Zhao, Characterization of *Komagataeibacter xylinus* by a polarization modulation imaging method, J. Phys. D: Appl. Phys. 53 (2019) 1.
28) X. Liu, B. Qiu, Q. Chen, Z. Ni, Y. Jiang, M. Long, and L. Gui, Characterization of graphene layers using super resolution polarization parameter indirect microscopic imaging, Opt. Express 22 (2014) 20446.
29) K. Ullah, X. Liu, M. Habib, and Z. Shen, Subwavelength Far Field Imaging of Nanoparticles with Parametric Indirect Microscopic Imaging, ACS Photonics 5 (2018) 1388.
30) Edward Collett. Field Guide to Polarization (SPIE, 2005).
31) P. Gupta, N. Gupta, and P. Dey, Morphometric analysis of endometrial cells in liquid-based cervical cytology samples, Cytopathology 28 (2016) 140.
32) H. Komagata, T. Ichimura, Y. Matsuta, M. Ishikawa, K. Shinoda, N. Kobayashi, and A. Sasaki M.D., Feature analysis of cell nuclear chromatin distribution in support of cervical cytology, J. Med. Imaging 4 (2017) 1.
33) D. Zink, A. H. Fischer, and J. A. Nickerson, Nuclear structure in cancer cells, Nat. Rev. Cancer 4 (2004) 677.